Preserving the Insulating Character and Tuning the Magnetic Properties through the Formation of Defects at NiFe2O4(001) Surfaces

Kedar Sharma, Lionel Calmels, Rémi Arras

Preserving the insulating character and tuning the magnetic properties through the formation of defects at $NiFe_2O_4$(001) surfaces

Kedar Sharma, Lionel Calmels, and Rémi Arras*

CEMES, Université de Toulouse, CNRS, 29 rue Jeanne Marvig, F-31055, Toulouse, France

E-mail: remi.arras@cemes.fr

Abstract

We performed a numerical investigation of the possible atomic and electronic reconstructions at the $NiFe_2O_4(001)$ surfaces. Using *ab initio* thermodynamics calculations, we identified that, $Ni_xFe_yO_8$-terminated surfaces can be stabilized in oxygen-rich conditions and are expected to be obtained with growth temperatures below 950 K. The stabilization of the $Ni_2Fe_2O_8$ termination obtained from a truncation of the bulk structure ends up in a slight reduction of the surface magnetization because of the transfer of holes at the surface, as a consequence of the polar character of the $NiFe_2O_4(001)$ layer. The associated surface states are expected to present a small band gap of 0.21 eV at the Fermi level, resulting from a charge ordering, which could disappear at high temperature to the benefit of the appearance of a spin-polarized two-dimensional hole gas. However, we demonstrated that the appearance of such a two-dimensional hole gas is subject to the conditions that the cation ordering in octahedral sites is not modified and that the stoichiometry is preserved. In particular, we highlighted that the formation of oxygen vacancies is expected to be easier at the surface and may help to recover the surface insulating state. According to our results, the surfaces stabilized in iron-rich or oxygen-poor conditions should present a higher magnetization.

Introduction

Spinel ferrites, MFe_2O_4, are promising materials for numerous applications ranging from medicine and catalysis to electronics and spintronics.[1–6] As for catalytic materials,[7–10] the constituents of electronic and spintronic non-volatile memories, such as magnetic tunnel junctions[2,3] or resistive switching devices,[11–13] are mainly functionalized through their surfaces or interfaces. The control of the structural and chemical properties of their interfaces is thus often considered as the ultimate key to successfully miniaturize and to improve the efficiency and versatility of these devices.

Complex bulk oxides crystallizing within the spinel structure possess a distorted face-

centered cubic sublattice of oxygen atoms in which mixed-valence cations occupy tetrahedral (Td) and octahedral (Oh) atomic sites. In $M\mathrm{Fe_2O_4}$ spinel ferrites, the M^{2+} and $\mathrm{Fe^{3+}}$ cation distribution among Td and Oh sites depends both on the chemical nature of the M^{2+} divalent cations and on the experimental growth conditions; it is characterized by the inversion degree λ ($0 \leq \lambda \leq 1$) according to the chemical formula $[M^{2+}_{1-\lambda},\mathrm{Fe}^{3+}_{\lambda}]_{\mathrm{Td}}[M^{2+}_{\lambda},\mathrm{Fe}^{3+}_{2-\lambda}]_{\mathrm{Oh}}\mathrm{O}^{2-}_{4}$. Along the [001] direction, the periodicity of the spinel structure thus corresponds to a succession of 4 $\{[M_{1-\lambda},\mathrm{Fe}_{\lambda}]_{\mathrm{Td}}\}^{(2+\lambda)+}/\{[M_{\lambda},\mathrm{Fe}_{2-\lambda}]_{\mathrm{Oh}}\mathrm{O}_4\}^{(2+\lambda)-}$ atomic bilayers (respectively called A/B in the following). Such materials are considered as polar.[14,15] Not surprisingly, changes of the physical properties have been reported in spinel ferrites thin films, compared to their bulk counterparts. Tentative explanation has been proposed, based on the formation of structural defects and on the contribution of the interfaces and surfaces, eventually considering their polar character.

$\mathrm{NiFe_2O_4}$ is a well-known member of the spinel-ferrite family, which displays an insulating behavior and a ferrimagnetic ordering with a high Curie temperature of 850 K. Its bulk ground state corresponds to a so-called inverse cation distribution ($\lambda = 1$), which means that Td sites are only occupied by $\mathrm{Fe^{3+}}$ cations. The $M^{2+}/\mathrm{Fe^{3+}}$ cation distribution in Oh site can be more difficult to control, but different experimental studies succeeded in stabilizing and measuring an ordered distribution corresponding to the space group $P4_122$ (No. 91),[16,17] which was also confirmed by numerical calculations as being the most stable distribution.[18,19] In (ultra-) thin films, different variations of the conductivity and magnetic properties have been reported. For example, Lüders, *et al.*[20] studied the thickness effect of $\mathrm{NiFe_2O_4}$ thin films grown by radio-frequency sputtering on a $\mathrm{SrTiO_3}$ substrate: they measured an enhancement of the spin magnetization of nearly 250% with the appearance of a metallic character when the thickness is decreased down to 3 nm, which they explained in terms of a lowering of the cation inversion parameter λ down to 0.83, and in terms of the significant role of the interface. In thin films with thicknesses of hundreds of nm grown by PLD, Anjum, *et al.*,[21] also found an increase of the electric conductivity, but they measured a reduction of the

magnetization to between 0.4 and 40% of the bulk value, the latter being measured for the samples grown with the highest values of the oxygen pressure. To explain these variations of properties, they highlighted the formation of lower-valent Ni cations, which may result from the formation of atomic vacancies. More recently, Nonaka, *et al.*,[22] evidenced the formation of magnetically-dead layers in $NiFe_2O_4(111)$ thin layers grown on $Al_2O_3(111)$ substrates, which they attributed to the formation of Fe_{Td} vacancies [$V(Fe_{Td})$].

To summarize, $NiFe_2O_4$ thin films can display an increase of their conductivity and different and opposite variations of their magnetic properties. To understand these modifications of their physical properties, several hypotheses have been proposed in terms of changes in their atomic structure, like the formation of structural defects or the modification of the inversion degree. If the contribution of the surfaces and interfaces is also mentioned, their influence on the formation of defects remains unclear. Interestingly $V(Fe_{Td})$ vacancies, which have been predicted to be unstable in bulk $NiFe_2O_4$,[19] are often considered as probable defects in $NiFe_2O_4$ thin films.[20,22] This discrepancy between bulk and thin films can partly be explained by possible surface/interface reconstructions, with the relaxation of surface Fe_{Td} atoms into the nearest B layers.[9,23] Moreover, the polar character of $NiFe_2O_4$ gives rise to a charge discontinuity at its surfaces or interfaces: electronic[15,24] or atomic reconstructions[23,24] are thus likely to happen.

In this study, we calculated from first-principles the formation energy of (001) $NiFe_2O_4$ surfaces, considering different atomic terminations in order to identify the most stable ones. These atomic terminations differ mostly by the presence of ordered atomic defects (atom vacancies, substitutions, exchanges), which may be more stable at the surface than in the bulk compound. In this paper, we will first explain how the experimental growth conditions should be adjusted to target specific terminations. In a second step, we will describe and explain the electronic and magnetic properties corresponding to the most stable atomic terminations which are relevant for the possible technological applications. In particular, we will show that the surface termination can preserve or suppress the insulating character

of bulk $NiFe_2O_4$, and eventually achieve the formation of spin-polarized two-dimensional electron or hole gases located at the surface. We will also describe which surface terminations should be favored to increase the spin magnetization of a thin film.

Methodology

To study the (001) $NiFe_2O_4$ surfaces, we performed first-principles calculations based on the density functional theory (DFT), using the VASP code[25,26] and the projector augmented wave (PAW) method.[27] The exchange-correlation potential was approximated thanks to the functional proposed by Perdew, Burke, and Ernzerhof and revised for solids (GGA-PBESol),[28,29] to which was added an on-site and rotationally-invariant $+U$ correction.[30] The effective U parameters were set equal to those used in our previous study on bulk $NiFe_2O_4$,[19] *i.e.* 4.0 eV and 2.5 eV, respectively for the Fe-3d and Ni-3d orbitals.

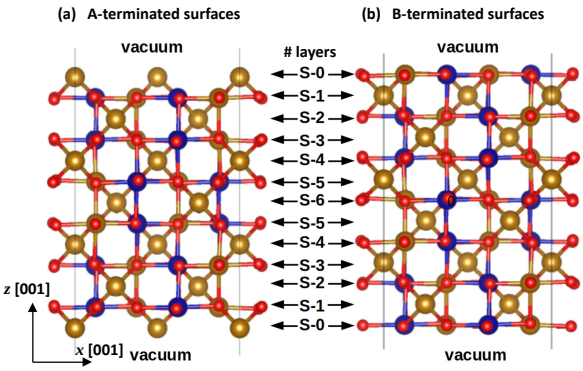

Figure 1: Schematic representation of the symmetric (001) slabs used for the calculations before any structural optimization with (a) two perfect A terminations and a chemical composition $Fe_2/[NiFeO_4]_2$ or (b) two B terminations, formed by a $[Ni_{Oh}Fe_{Oh}O_4]_2/Fe_2$ bi-layer. Ni, Fe, and O correspond to atoms in blue, brown, and red color, respectively.

The surfaces were modeled using slabs with a thickness of 13 (A or B) atomic layers, as shown in Fig.1. In the center of the slabs, we considered that $NiFe_2O_4$ crystallizes in a perfectly inverse spinel ($\lambda = 1$) and the Ni/Fe cation distribution was set to that of the ground-state structure with the space group $P4_122$. The continuity of the crystallographic spinel structure is preserved in the entire slabs. Only the chemical composition or cation

ordering in the surface bi-layer (S-0/S-1) was changed to generate 27 different (001) surface terminations (more details are given in Sec. S.I of the supplementary information). To study their stability, we chose to use symmetric slabs with two equivalent surface terminations, having $(\sqrt{2} \times \sqrt{2})R45°$ in-plane dimensions, according to the vectors of the spinel primitive cell; in other words, the dimension of these supercells is $a_0 \times a_0$, where $a_0 = 8.277$ Å is the fixed in-plane equilibrium lattice parameter, which was calculated for bulk $NiFe_2O_4$ with a conventional cubic cell of 56 atoms. Each A/B (001) bilayer of this cubic cell thus contains 2 formula units (f.u.) of $NiFe_2O_4$. The first Brillouin zone was sampled by a Monkhorst-Pack grid[31] of $6 \times 6 \times 1$ $\boldsymbol{k}$ vectors. A vacuum layer with a thickness of at least 15 Å has been added to avoid any spurious interaction between the periodically repeated surfaces. The atomic positions and the out-of-plane lattice parameter have been optimized by minimizing the internal forces.

Schematic representations of the atomic structures have been plotted with the VESTA software[32] and the band structures have been post-processed with the PyProcar package.[33]

Results

Thermodynamic stability and atomic reconstructions

Thermodynamic stability

We first investigated the thermodynamic stability of $NiFe_2O_4(001)$ surfaces as a function of their atomic termination. According to Fig. 1, cutting a perfect $NiFe_2O_4$ bulk crystal can lead to two different (001) surfaces, which either correspond to a perfect A termination or to a perfect B termination. In the following, the surface terminations are labelled by the chemical composition of their surface (S-0) and subsurface (S-1) atomic layers: (S-0)/(S-1) = $[Fe_2]_{Td}/[Ni_2Fe_2]_{Oh}O_8$ for the perfect A termination, while (S-0)/(S-1) = $[Ni_2Fe_2]_{Oh}O_8/[Fe_2]_{Td}$ for the perfect B termination. It is also understood that because of the dangling bonds, the

oxygen octahedra are changed to square pyramids (Py) and the cations initially located in tetrahedra can be seen as bridge adatoms; for the sake of simplicity, we will continue to write octahedra or tetrahedra. In addition to the two perfect surface terminations obtained from a direct truncation of the bulk structure, we have generated 25 additional surface terminations (of which the list is given in Fig. S1) by substituting, removing or swapping cations, or by creating oxygen vacancies in these perfect surfaces. We systematically calculated their formation energy γ per surface area A, which can be expressed as a function of the ground state energy E^{slab} of each cell and of the chemical potentials μ_i and numbers of atoms n_{i} inside the cell, i = Ni, Fe, O being the chemical species constituting the slab:[34–36]

$$\gamma = \frac{E^{\text{slab}} - n_{\text{Ni}}\mu_{\text{Ni}} - n_{\text{Fe}}\mu_{\text{Fe}} - n_{\text{O}}\mu_{\text{O}}}{2A} \tag{1}$$

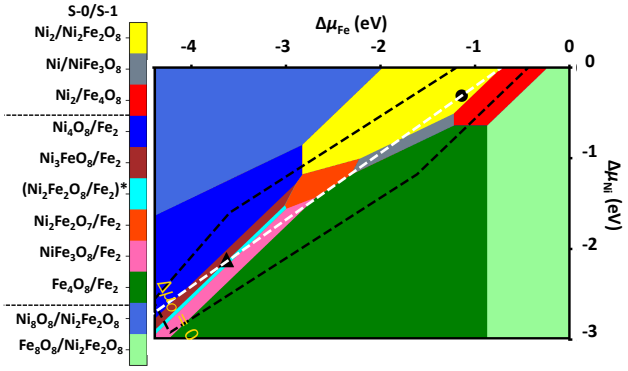

Figure 2: Phase diagram displaying the most stable (001)$NiFe_2O_4$ surface terminations as a function of the variations of chemical potentials $(\Delta\mu_{\text{Fe}}, \Delta\mu_{\text{Ni}})$. The area delimited by the black dotted lines corresponds to the stability domain of the bulk crystal.[19] The black triangle [of coordinate $(\Delta\mu_{\text{Fe}}, \Delta\mu_{\text{Ni}}, \Delta\mu_{\text{O}}) = (-3.63, -2.12, -0.50)$] and black circle $[(-1.13, -0.31, -2.20)]$ are used to illustrate oxygen-rich and oxygen-poor growth conditions, respectively.

It is customary to plot the surface-stability phase diagram (Fig. 2) as a function of the difference $\Delta\mu_i$ between the chemical potential μ_i of the chemical species i and the total energy per atom E_i^{elem} of the same chemical species in its pure elemental phase: $\Delta\mu_i = (\mu_i - E_i^{\text{elem}})$. We have considered the stability of surfaces at equilibrium both with a O_2 gas reservoir located above the surface and with the infinite bulk $NiFe_2O_4$ oxide below it.[35] In other

words, we are interested in finding the surface terminations which are stable in the range of chemical potentials delimited by the black dashed lines in Fig. 2, which corresponds to the experimental conditions which would allow the growth of bulk $NiFe_2O_4$ and avoid the formation of competing phases, as already calculated in our previous work.[19]

From Fig. 2, we conclude that among the 27 surface terminations considered in our calculations (see Fig. S1), 9 terminations only can become the most stable ones and fulfil the chemical-potential criteria for the bulk $NiFe_2O_4$ to be stable. None of these surfaces corresponds to the perfect A or B termination [As discussed later, the termination $(Ni_2Fe_2O_8/Fe_2)$* has the same stoichiometry as the perfect B termination, but a different cation ordering inside the Oh sublattice at the S-0 layer]. Two other surfaces, namely $Ni_8O_8/Ni_2Fe_2O_8$ and $Fe_8O_8/Ni_2Fe_2O_8$, could also be stabilized for growth conditions beyond these criteria, with small values of $\Delta\mu_{\mathrm{Ni}}$ and $\Delta\mu_{\mathrm{Fe}}$; these two surface terminations would correspond to the formation of a full NiO(001) or FeO(001) atomic layer on top of a B-terminated $NiFe_2O_4$ surface. According to Fig. S1, we can also see that, in addition to the most stable surface terminations, 4 other surfaces display energies close to the most stable ones (with a surface energy less than 80 meV/Å^2 above that of the most stable terminations, for at least one of the two growth conditions represented in Fig. 2) and may thus be metastable, i.e. likely to be grown in out-of-equilibrium conditions. The physical properties of the above mentioned 12 selected surfaces are summarized in Table 1. Interestingly, we can see that 5 of these terminations ($Ni_2/Ni_2Fe_2O_8$, $Ni/NiFe_3O_8$, $Ni/Ni_2Fe_2O_8$, $Ni_2Fe_2O_7/Fe_2$ and Fe_4O_8/Fe_2) present a variation of their formation energy between the two selected chemical potentials which is of less than 20 meV/Å^2, suggesting that their stability is robust and may be quasi-independent on the experimental growth conditons.

To get a better insight in the relations between the growth conditions and the stabilization of a specific surface termination, it is possible to express the oxygen chemical potential $\Delta\mu_{\mathrm{O}}$ entering in the calculation of the surface energies, as:[34,37]

Table 1: Summary of the different physical and chemical properties calculated for the 11 most stable surface terminations: surface formation energy γ, charges Q carried by the surface (S-0) and subsurface (S-1) atomic layers before and after the electronic reconstruction associated to the charge transfer ΔQ (positive/negative values corresponding holes/electrons; see more details in the text), work function ϕ, conducting state (metallic M or insulating I), total spin magnetic moment integrated over 3 atomic A/B bilayers (from S-0 to S-5) of 2 f.u. of $NiFe_2O_4$ and variation of total spin magnetic moment according to the bulk value $\Delta M = M_{\mathbf{at.+elec.}} - 12$.

Surface termination S-0/S-1	γ (meV/Å^2) O-poor	O-rich	Q_{S-0}/Q_{S-1} (e/2 f.u.) atomic	at.+elec.	ΔQ (e/2 f.u.)	Φ (eV)	Conductivity (M/I)	M (μ_B/6 f.u.) atomic	at.+elec.	ΔM (μ_B/6 f.u.)
A terminations										
Ni_2/Fe_4O_8	77	114	$4+/4-$	$2+/4.5-$	$-2 \rightarrow 2Ni_{Td}$, $-0.5 \rightarrow 2Fe_{Oh}$,$-0.5 \rightarrow 1Fe_{Oh}$(S-3)	4.21	M	24	24.63	+12.63
$Ni_2/Ni_2Fe_2O_8$	74	90	$4+/6-$	$3+/6-$	$-1 \rightarrow 2Ni_{Td}$	4.31	M	18	19	+7
$NiFe/Ni_2Fe_2O_8$	76	102	$5+/6-$	$3+/6-$	$-1 \rightarrow Fe_{Td}$, $-1 \rightarrow Ni_{Td}$	4.43	I	15	17	+5
$Ni/NiFe_3O_8$	78	78	$2+/5-$	$1.5+/5.5-$	-0.5: $Ni_{Oh} \rightarrow Ni_{Td}$	4.92	I	23	23	+11
$Ni/Ni_2Fe_2O_8$	87	77	$2+/6-$	$2.5+/5.5-$	$+1 \rightarrow Ni_{Td}$+$2Ni_{Oh}$	5.30	I	20	19	+7
B terminations										
$Ni_2Fe_2O_7/Fe_2$	84	72	$4-/6+$	$3-/6+$	$+1 \rightarrow Ni_{Oh}$	5.57	I	12	11	-1
Fe_4O_8/Fe_2	87	70	$4-/6+$	$3-/6+$	$+1 \rightarrow 2Fe_{Oh}$	5.50	M	18	17	+5
$NiFe_3O_8/Fe_2$	93	67	$5-/6+$	$3-/6+$	$+1 \rightarrow Fe_{Oh}$, $+1 \rightarrow Ni_{Oh}$	5.69	I	15	13	+1
$(Ni_2Fe_2O_8)^*/Fe_2$	102	66	$6-/6+$	$3-/6+$	$+1 \rightarrow 2Fe_{Oh}$, $+2 \rightarrow 2Ni_{Oh}$	5.78	I	12	9	-3
$Ni_2Fe_2O_8/Fe_2$	103	67	$6-/6+$	$3-/6+$	$+1 \rightarrow 2Fe_{Oh}$, $+2 \rightarrow 2Ni_{Oh}$	5.77	$\sim$ M	**12**	9	-3
Ni_3FeO_8/Fe_2	112	65	$7-/6+$	$4-/6+$	$+3 \rightarrow 3Ni_{Oh}$, $+1 \rightarrow Ni_{Oh}$(S-2)	5.85	I	9	5	-7
Ni_4O_8/Fe_2	123	67	$8-/6+$	$4-/6+$	$+4 \rightarrow 4Ni_{Oh}$, $+1 \rightarrow 2Ni_{Oh}$(S-2)	5.90	I	6	1	-11

$$\begin{aligned}\Delta\mu_O(T,P) =& \frac{1}{2}\{[H_0 + \Delta H(T)] - T\,[S_0 + \Delta S(T)]\} \\ &+ \frac{1}{2}k_B T \ln(\frac{p}{p_0})\end{aligned} \tag{2}$$

where $\Delta H(T) = C_p\,(T - T_0)$, $\Delta S(T) = C_p \ln(T/T_0)$. $H_0 = 8.7$ kJ mol^{-1} and $S_0 = 205$ J mol^{-1} K^{-1} are tabulated values.[37,38] We used $C_p = 3.5k_B$ for the constant-pressure heat capacity per diatomic molecule and $p_0 = 1$ atm and $T_0 = 298$ K as the standard pressure and temperature. Considering the sets of chemical potentials $(\Delta\mu_{Fe}, \Delta\mu_{Ni})$ associated to the white dashed line in Fig. 2 and corresponding to the surface formation energies given in Fig. S2, we used Eq. 2 to plot in Fig. 3 a phase diagram of the most stable surface terminations as a function of the growth temperature T and oxygen partial pressure p.

As expected, it can then be seen that stabilizing A-like-terminated surfaces will preferably require oxygen-poor conditions, i.e. low p and high T. According to our calculations, such

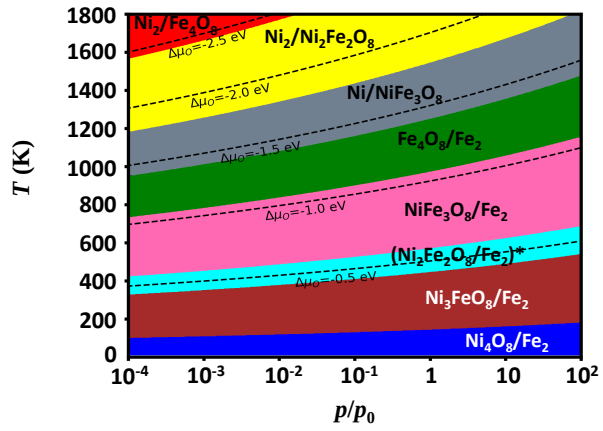

Figure 3: More stable (001)$NiFe_2O_4$ surface terminations as a function of the growth temperature T and the oxygen partial pressure p.

surfaces would indeed require temperatures higher than 954 K for $p/p_0 > 10^{-4}$, which is far from the growth conditions generally used for synthesizing such materials.[39] For temperatures lower than 954 K, we will mostly stabilize B-like-terminated surfaces. The lower $\Delta\mu_O$ is, the higher the ratio between the number of Ni atoms over the number of Fe atoms is. The predominance of Ni over Fe cations near surfaces cannot however be asserted with precision: the results given in Fig. 3 are indeed mostly qualitative as there is not a unique set of $(\Delta\mu_{Fe}, \Delta\mu_{Ni})$ corresponding to a specific value of $\Delta\mu_O$ and because, as mentioned previously, several surface terminations have very close formation energies. Our calculations nonetheless tend to predict a higher stability of B-like $NiFe_2O_4$ surface termination. As explained later in more details, the perfect B surface ($Ni_2Fe_2O_8/Fe_2$), absent in Fig. 3, could be stabilized through the formation of oxygen vacancies or after a Ni/Fe cation re-distribution inside the octahedra sublattice.

It is interesting to compare our results with those reported for the (001) surfaces of the half-metallic magnetite Fe_3O_4, which has extensively been studied, both theoretically and experimentally. As we calculated for $NiFe_2O_4$, B-terminated surfaces have generally been found more stable for the Fe_3O_4 oxide. For this compound, it has however been demonstrated that iron-rich surfaces with a A-like termination can be synthetized by properly selecting the suitable growth conditions.[40,41] Such surfaces have however been found metastable and

annealing the sample induces a re-oxidization of the surface with a recovering of a B-type termination.[40] In iron-rich conditions, calculations have also shown the possibility to stabilize a surface termination by localizing Fe adatoms in vacant octahedra sites where they form dimers, when the excess of iron corresponds to a full A monolayer.[41] This formation of dimers has been confirmed but becomes unstable when the temperature is increased, leading to the diffusion of the additional Fe atoms into the bulk, or when the surface is exposed to O_2, inducing the appearance of Fe_xO_y clusters,[42] in agreement with the earlier reported formation of a FeO(001) layer at high Fe content.[41] Considering these results on the Fe_3O_4 surfaces, we calculated the surface formation energy corresponding to the appearance of Ni ($Ni_4Fe_2O_8/Fe_2$ termination) or Fe ($Ni_2Fe_4O_8/Fe_2$) dimers at the B-type surface, but we found that such terminations are less stable than their A-terminated counterparts, $Ni_2/Ni_2Fe_2O_8$ and $Fe_2/Ni_2Fe_2O_8$ respectively (see Fig. S1). Owing to this first discussion, we can thus consider that $NiFe_2O_4$ A-like surface terminations, even if less probable than B-like surfaces, could also be grown under appropriate growth conditions.

Secondly, it is interesting to point out that the perfect B termination ($Ni_2Fe_2O_8/Fe_2$) that we propose corresponds to the distorted bulk truncation (DBT) model which was considered in the early studies of $Fe_3O_4(001)$ surfaces.[43] In 2014, a more complex atomic reconstruction was proposed and observed for Fe_3O_4; it is referred as the subsurface cation vacancy (SCV) structure, which consists of the simultaneous creation of 2 Fe(Oh) vacancies in the S-2 atomic layer and of 1 Fe(Td) interstitial in the S-1 layer, equivalent to the appearance of a $Fe_{11}O_{16}$ phase[44] and consistent with the formation of Koch-Cohen defects in bulk $Fe_{1-x}O$ oxide.[4,45] Such a surface model would be more difficult to calculate for a ternary compound like $NiFe_2O_4$ and has consequently not been considered in this paper.

Finally, the possible formation of a full NiO or FeO(001) atomic layer has already been discussed with Fig. 2. Such terminations may indeed appear to be stable, but chemical-potential values outside of the ranges for the stabilization of bulk $NiFe_2O_4$ crystals. The boundaries between the different domains remain nonetheless relatively close one from each

other and the possibility of growing such a surface cannot however be totally discarded; this is particularly true in the case of the NiO layer for which the domain boundary is close to the bulk one for a large range of oxygen chemical potentials, on the contrary to FeO, which would require both oxygen-poor and iron-rich conditions to be grown. It is moreover important to note that the presence of rock-salt NiO phases has already been reported near antiphase boundaries in $NiFe_2O_4$[46] and that the formation of a $NiFe_2O_4$-like film was successfully demonstrated through the diffusion of Ni atoms at the Fe_3O_4/NiO interface.[47]

To explain the stability of the surfaces as a function of their chemical composition and to understand their physical properties, we will discuss in the next sections their corresponding atomic and electronic structures. $NiFe_2O_4$(001) layers being polar,[14] the localization of compensation charges can happen due to electronic reconstructions, to avoid a divergence of the polar electrostatic field or due to the presence of defects,[15] in order to help stabilizing the surfaces.

Surface atomic relaxations

In this section, we will describe the atomic relaxations induced by the surfaces.

In Fig. 4(a) and (b), we show how the atomic structure is modified in the vicinity of the surfaces. For a A-terminated surface, with the $Ni_2/Ni_2Fe_2O_8$ termination for example [see Fig. 4(a)], the A layer at S-0 relaxes toward the subsurface B layer (S-1), in agreement with calculations performed on $Co_xNi_{1-x}Fe_2O_4$ surfaces.[9] Such a relaxation induces a lowering of the out-of-plane lattice parameter at the surface, by approximately 0.7 Å for the A-terminated surface, while the B-terminated surface presents spatial oscillations of the interlayer distance, with an amplitude lower than 0.1 Å [see Fig. 4(c)].

In addition to the lowering of out-of-plane lattice parameter, we can see from the (001) plane view that oxygen atoms are displaced to form pairs separated by narrower distances [represented by the green arrows in Fig. 4(a) and (b)] along the [−110] direction, these pairs being orientated perpendicularly to the chain of cations in octahedral sites. The O-O distance

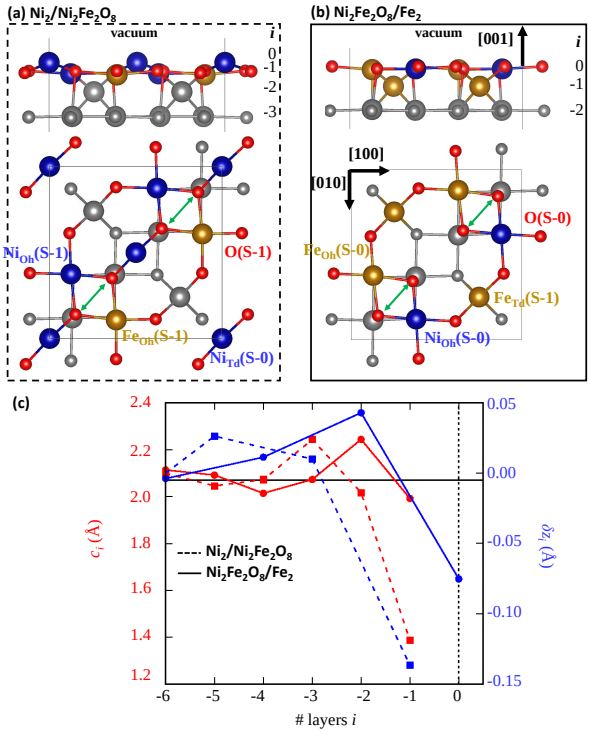

Figure 4: Optimized atomic structure near (a) a A-terminated surface with a $Ni_2/Ni_2Fe_2O_8$ atomic termination and (b) a B-terminated surface with a $Ni_2Fe_2O_8/Fe_2$ termination. The same color code as in Fig. 1 is applied to the surface bilayer, while subsurface layers are plotted in gray. (c) Layer-resolved out-of-plane lattice parameter $c_i = \langle z \rangle_{i+1} - \langle z \rangle_{i-1}$ and cation-oxygen rumpling $\delta z_i = \langle z(\mathrm{Ni, Fe}) \rangle_i - \langle z(\mathrm{O}) \rangle_i$ calculated for these two surfaces.

between oxygen atoms of these pairs is $\sim$ 2.4 Å(2.5 Å) for the B(A)-terminated surface, while the O-O distance is $\sim$ 2.8 Å in the less-distorted S-2 layer. These distortions in the B-terminated surface are a direct consequence of the broken bonds formed by the oxygen atoms which are only bonded to Fe_{Td} atoms of the S-1 layer. Still for the B-terminated surface, the average cation-oxygen bond length in the S-0 (001) atomic layer of the $Ni_2Fe_2O_8/Fe_2$ surface is decreased down to 1.917 Å, while it is of 2.031 Å in the S-2 layer, and the O-cation-O angles are of 82°/98° in the S$-$0 layer, while they are closer from 90°(88°/92°) in S$-$2. A similar Jahn-Teller distortion was already proposed to explain the stabilization of the $(\sqrt{2}\times\sqrt{2})R45°$ B-terminated (001) polar surfaces of magnetite Fe_3O_4,[43] without requiring the formation of a pattern of ordered defects such as oxygen or Fe_{Td} vacancies.[48–50] Analyzing more in detail these distortions, we also found that, according to the Fe-O bond lengths between Fe and O located in the same atomic layer, the two Fe atoms at the B(S-0) surface layer are not equivalent anymore. Indeed, while the Fe-O distances for both Fe atoms at the center of the slab (S-6) are equal in average to 2.02 Å, the averaged Fe-O distance is 1.90 Å and 1.97 Å, for the two surface Fe atoms, respectively.

Finally, from Fig. 4(c), we can see that both surfaces present the formation of a negative cation-oxygen rumpling of $\delta z_{\text{S-1}} = -0.14$ Å (A-terminated) and $\delta z_{\text{S-0}} = -0.075$ Å (B-terminated), which means that oxygen atoms are, in average, pulled outward of the surface, while cations are displaced in the opposite direction.

Electronic reconstructions

As written previously, $NiFe_2O_4$ is polar along the [001] direction. Consequently, electronic and/or atomic reconstructions are expected to appear according to the polar-catastrophe scenario.[15,51] In a (001) bi-layer containing 2 f.u. of $NiFe_2O_4$, $(Fe_2)_{Td}$ (A) and $Ni_2Fe_2O_8$ (B) atomic layers carry a charge Q of +6e or $-$6e, respectively.[4] To cancel the divergence of the electrostatic potential in asymetric layers, or to preserve the charge neutrality in the non-stoichiometric and symmetric slabs, the charge of the surface A or B layers should be

lowered down to half of its value in bulk $NiFe_2O_4$,[15,52] i.e. $Q_{\text{S-0}} = \pm 3e$ per 2 f.u., whatever the local stoichiometry imposed by the details of the surface termination.

In Table 1, we reported the theoretical charges ($Q_{\text{S}-0}/Q_{\text{S}-1}$ "*atomic*") that the surface and subsurface layers would carry if there was only atomic reconstructions but no additional charge compensation and if the charge of all the Ni, Fe and O ions was respectively of $2e$, $3e$ and $-2e$. In the same table, we also provide the charges ($Q_{\text{S}-0}/Q_{\text{S}-1}$ "*at.+elec.*") calculated from first principles, accounting for additional electronic rearrangement between ions within the slab. The next column of the table indicates how the additional charge $\Delta Q = Q(\text{atomic}) - Q(\text{at.+elec.})$ induced by the electronic reconstruction is distributed within the slab. These charge redistributions have been evaluated approximately, from the variations of the contribution of the different atoms to the density of states (DOS) (displayed in Fig. S3) and from the changes of spin magnetic moments.

In oxygen-poor(rich) growth conditions, the most-stable A(B)-terminated surfaces do not display any significant difference of formation energy, except for the $Ni/Ni_2Fe_2O_8$ termination; the predominance of a specific termination will mostly depend on the thermodynamic conditions.

In an oxygen-poor growth condition ($\Delta\mu_{\text{O}} = -2.2$ eV), the B-terminated surfaces, which are metastable, display on the contrary strong variations of their formation energies. We can in particular notice that the B surfaces are more stable when their Ni-content decreases and when the surface stoichiometry is the closest from fullfilling the requirement of a surface charge ($Q_{\text{S}-0}$ "*atomic*") of $-3e$, which minimizes the required additional charge redistribution. The more stable B-terminated surfaces under oxygen poor growth condition are those with a Fe_4O_8/Fe_2 termination (containing no Ni atoms) or with a $Ni_2Fe_2O_7/Fe_2$ termination (with an oxygen vacancy). The localization of the charges after the electronic reconstruction moreover depends on the difference between the number of charges to be distributed and the number of available host cations, i.e. Ni^{2+} to accomodate holes and Fe^{3+} for electrons according to the energy of their respective occupied and unoccupied bands. The surfaces with not

enough surface host cations, such as the $Ni/NiFe_3O_8$ and $Ni/Ni_2Fe_2O_8$ A-like terminations or the Ni_3FeO_8/Fe_2 and Ni_4O_8/Fe_2 B-like terminations are the least stable in O-poor or O-rich conditions, respectively and their electronic reconstruction will extend in subsurface layers as mentioned in Table 1 and in Fig. S3. How the minimization of the charge transfer may help the stabilization of a specific surface termination is difficult to assess, but it may not play a determinent role if compared to the choice of chemical potentials. For example, the surface termination $[Fe]^{3+}/[Ni_2Fe_2O_8]^{6-}$ (with a half A layer coverage), for which ΔQ vanishes, is not found among the most stable surfaces for the chosen set of chemical potentials, similarly to the results found for $Fe_3O_4(001)$ surfaces.[43]

The calculations presented in this study have been performed with a rather low surface area because of the technical constraints imposed by DFT calculations. The stabilization of surfaces with more complex atomic reconstructions and thus a larger in-plane periodicity cannot be ruled out and would minimize the transferred charge ΔQ. As discussed in the previous section, the present reconstructions appear nonetheless realistic in light of the experimental results from the literature obtained on Fe_3O_4, for example.

Surface electronic and magnetic properties

We will now discuss the consequences of the atomic and electronic reconstructions, described in the previous section, on the functional properties of $NiFe_2O_4$.

Work function

The charge reconstruction gives rise to a compensating charge $Q_{\text{S-0}}$ at the surface layer S-0, which depends on the surface termination and modifies the work function ϕ. Similarly to what is known for perovskite compounds, positively-charged (A-terminated) surfaces have a lower work function than the negatively-charged (B-terminated) ones.[53] The 2 A-terminated surfaces in Table 1, which have a full Ni_{Td} coverage, have work functions between 4.2 and 4.3 eV. ϕ increases up to 5.3 eV for the half-full $Ni_{0.5}$ terminations, when charges start to be

transferred into the B subsurface layer (S-1). The work function of the B-terminated surfaces increases from 5.50 eV to 5.90 eV as we increase the Ni atom content at the detriment of Fe atoms. This increase of ϕ is consistent with the increasing number of transferred holes, from $+1e$ to $+5e$, which will have the effect of lowering the Fermi energy.

Electronic structure and two-dimensional electron gases

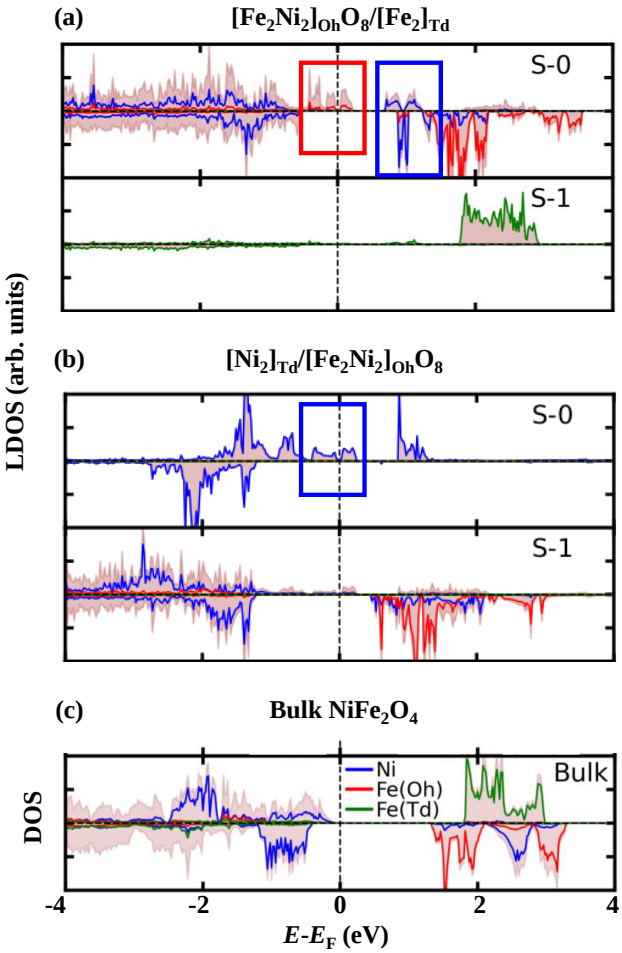

Figure 5: Layer-resolved density of states calculated for a surface with a (a) B-like $Ni_2Fe_2O_8/Fe_2$ and (b) a A-like $Ni_2/Ni_2Fe_2O_8$ terminations. (c) The projected DOS of bulk $NiFe_2O_4$ is given for comparison. Positive and negative DOS values correspond to majority- and minority-spin projections, respectively.

The bulk inverse spinel $NiFe_2O_4$ crystal is insulating with a calculated fundamental band

gap of 1.34 eV.[19] The valence-band maximum (VBM) belongs to the majority-spin channel and mostly involves Ni_{Oh}-d+O-2p orbitals, while the conduction-band minimum (CBM) is in the minority-spin channel with Fe_{Oh}-d contributions. For certain terminations, we idendified from the layer-resolved DOS (LDOS) of Fig. S3 that the charge reconstruction can lead to a conductive surface, with a localized spin-polarized two-dimensional electron or hole gas, as already proposed for spinel/spinel interfaces.[24] Indeed, as it can be seen in Table 1, the surface terminations for which one transferred electron is shared by two atoms of the same chemical species become metallic; the only exception is the $Ni/Ni_2Fe_2O_8$ termination, which remains insulating; the band gap for the S-1 layer is however strongly lowered, down to 0.21 eV in this case.

For a perfect B termination, 3 holes/2 f.u. are transferred to the surface layer [Fig. 5(a)]: 1 hole will localize on each of the two Ni^{2+} cations, turning them into Ni^{3+} cations, both holes contributing to the unoccupied Ni-$d_{x^2-y^2}$ surface states corresponding to the bands with energies between $\sim$ 0.6 and $\sim$ 1.2 eV above the Fermi level; the last hole, corresponding to the bands of energies $\sim$ 0.1-0.2 eV above the Fermi level, is shared between the two Fe_{Oh} and the surrounding oxygen atoms. Roughly, we can consider that these two surface Fe cations change their oxidation state to the unusual value of $Fe^{3.5+}$. If we allow these two atoms to relax independently, a charge ordering appears due to structural distortions described previously, leading to the opening of a small direct band gap of 0.21 eV at the X point [Fig. 6(a)]. The corresponding charge dispropornation can be regarded as a $2d^{3.5+} \rightarrow d^{3+} + d^{4+}$ Mott transition. More precisely, the unoccupied band above the Fermi level involves hybridization between $d_{x^2-y^2}$ and $(p_x + p_y)$ orbitals and because of the strong contribution of the O-p orbitals, this state can rather be described by a partial ligand hole state $d^{5+\delta}\underline{L}^{1-\delta}$, as already proposed in other Fe-based oxides.[54] As shown in the charge density of Fig. 6(a), this hole spreads over the surface Fe atom displaying the lowest Fe-O distances and its four surrounding oxygen first neighbors, reducing its spin magnetic moment by 0.3 μ_B. If the two Fe cations of the B surface are fixed to be equivalent, the

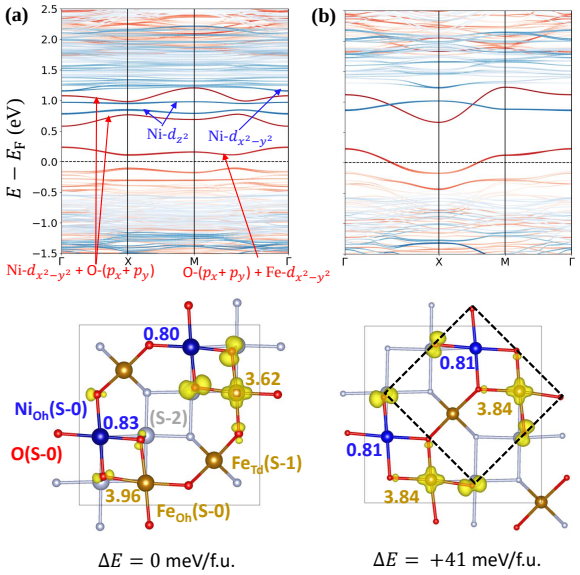

Figure 6: Band structure of the perfect B surface with a $Ni_2Fe_2O_8/Fe_2$ termination, calculated for (a) the $(\sqrt{2} \times \sqrt{2})R45°$ conventional surface with the dimension $a_0 \times a_0$ and containing 2 formula units of $NiFe_2O_4$ and (b) the primitive cell containing 1 formula unit (as delimited by the black dotted lines in the bottom structure). In the subfigure (a), the high-symmetry points of the Brillouin zone of the conventional cell have the reduced coordinates $X(1/2, 0, 0)$ and $M(1/2, 1/2, 0)$; in subfigure (b), the high-symmetry points $X(1/2, 1/2, 0)$ and $M(1/2, 0, 0)$ have been oriented to get Bloch vectors along the same crystallographic axes as in subfigure (a). In the band structures, red and blue bands represent the majority- and minority-spin projections and the intensity of the plots highlights the contribution of the surface atoms. The calculated top-view surfaces are shown at the bottom, with the yellow surfaces representing the partial charge densities calculated for the unoccupied bands of energies between E_F and $E_F + 0.45$ eV. The blue and brown values correspond to the spin magnetic moments (in μ_B) of Ni and Fe cations, respectively. The relative total energy ΔE shows that the surface (a) is more stable.

charge ordering will not occur and the calculated hole band will cross the Fermi level, leading to the formation of a two-dimensional hole gas, with an effective mass at Γ of 2.14 m_0 along the $\Gamma_{\rightarrow X}$ direction (parallel to the Fe_{Oh}-O chemical bonds) and of 4.09 m_0 along the $\Gamma_{\rightarrow M}$ direction [Fig. 6(b)]. This second surface configuration (for which surface Fe cations are equivalent) is however found 82 meV/2 f.u. less stable than the surface which allows a charge ordering. Nonetheless, it cannot be excluded that the perfect B surface can become conductive at high temperature, when the consequences of electronic correlations are less important[55] and/or when more disorder is present.[56]

As it can be seen in Fig 5(b), the $Ni_2/Ni_2Fe_2O_8$-terminated surface is predicted to be metallic, due to the $\Delta Q = -1e$ charge transferred to the two Ni^{2+}_{Td} cations. Because of the distance between these two Ni^{2+}_{Td} cations, we can observe, on the DOS curve, the formation of a quasi-band gap, with the crossing of dispersive $d_{x^2-y^2}$ bands at the Fermi level, characteristic of a semi-metallic character. The effective mass of the holes in the bands at the Fermi level is of 2.12 m_0 along the $\Gamma_{\rightarrow X}$ direction and of 1.35 m_0 along the $\Gamma_{\rightarrow M}$ direction.

In this section, we have shown that, for both the perfect A or B terminations, the transferred charges are well localized at the surface and could lead to the generation of two-dimensional electron or hole gases, with small effective masses along in-plane directions and with a spin polarization of +100%, which could be interesting for spintronic applications.

Surface spin magnetization

The calculated total spin magnetic moment of bulk $NiFe_2O_4$ is of to 2 μ_B/f.u., which agrees with the theoretical value expected for a ferrimagnetic ordering (with an antiferromagnetic coupling between cations in Td and Oh sites) and a magnetic moment of 2 μ_B for Ni^{2+} and 5 μ_B for Fe^{3+} cations.

In every calculated surface, we found that the ferrimagnetic ordering is globally preserved. As discussed in Sec. S.III of the supplementary information, the magnetic ordering is however more complicated in the presence of surface interstitial atoms or when a full FeO or NiO

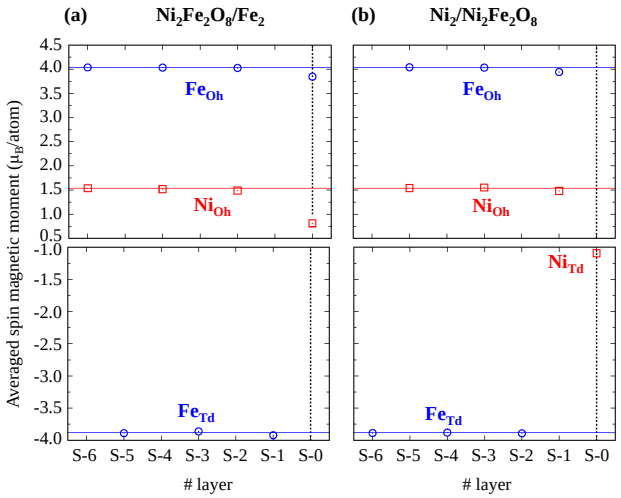

Figure 7: Averaged spin magnetic moments per atom near the (a) B-terminated ($Ni_2Fe_2O_8/Fe_2$) or (b) A-terminated ($Ni_2/Ni_2Fe_2O_8$) surface.

monolayer is added.

In agreement with a previous study on the consequences of structural defects in bulk $NiFe_2O_4$,[19] the variations of magnetic moments at the surface can be understood and decomposed as a sum of an *atomic* (i.e. before the electronic reconstruction) and an *electronic* (i.e. after the electronic reconstruction) contributions (see Table 1). From the LDOS discussed in the previous section, we have shown that the electronic structure can be drastically affected at the surface, which can even become metallic. Due to the modification of their oxidation states, the spin magnetic moment of the cations will also change.

For the perfect B termination $Ni_2Fe_2O_8/Fe_2$, we calculated a local decrease of the total spin magnetic moment of 3.0 μ_B, which is independent of the presence or not of the charge ordering. This variation is strongly localized at the surface layer and can be related to the localization of the 3 holes during the electronic reconstruction. These 3 holes are associated with the 3 unoccupied majority-spin surface bands (shown with red lines) in Fig. 6(a), which is consistent with the decrease of the averaged spin magnetic moment of the Fe_{Oh} and Ni_{Oh} surface atoms (atomic layer S-0) by 0.24 and 0.73 μ_B, respectively, as displayed in Fig. 7(a).

Concerning the $Ni_2/Ni_2Fe_2O_8$ A-terminated surface, the 2 surface Ni cations display a magnetic moment of $\simeq$ 1.1 μ_B (in absolute value) lower than their bulk counterpart of

$\simeq 1.5\ \mu_B$ (in Oh sites far from the surface) [see Fig. 7(b)]. This decrease of the spin magnetic moment is consistent with the transfer of 1 electron in the minority-spin bands. Nonetheless, the calculated total spin magnetic moment increases by $+7\ \mu_B/2$ f.u. compared to the bulk value; this increase mostly has an atomic origin and is governed by the substitution of the Fe_{Td} by Ni_{Td} atoms at the surface.

More generally, the calculated moments reported in Table 1 show that, among the 12 most stable surfaces, only 5 terminations (mostly corresponding to the Ni_{Oh}-rich B-terminated surfaces) will show a lowering of the spin magnetic moment, which conversely increases for all the other surfaces. Our calculations thus suggest that the excess of Ni_{Td} atoms at the A-terminated surfaces stabilized under oxygen-poor growth conditions could partially be considered as an explanation of the large spin magnetizations measured for $NiFe_2O_4$ surfaces.[20,57,58] According to our calculations, such surfaces could be stabilized due to a local lowering of the inversion degree ($Ni/NiFe_3O_8$ or Ni_2/Fe_4O_8), but also due to substitutions of the Ni atoms at the surface ($Ni_2/Ni_2Fe_2O_8$). On the contrary, the excess of Ni_{Oh} atoms at B-terminated surfaces stabilized under oxygen-rich growth conditions lower the spin magnetization. The spin magnetic moments per atom calculated for the 12 most stable surfaces are provided as supplementary materials in Fig. S4.

As shown in Table S1, if a NiO layer formed at the surface, it would display an antiferromagnetic ordering with a zero net magnetization, which would result in a decay of the layer magnetization.

Stability of defects

In the previous sections, we analyzed the atomic and electronic properties of the perfect B-terminated surface. We also discussed the evolution of these physical properties for other B-terminated surfaces obtained by subsequent Fe/Ni substitutions, and also for A-type surfaces, which can be viewed as B surfaces decorated with metallic adatoms. In this last section, we will now explain which effects could be expected from different cation distributions or in

the presence of atomic vacancies, as these defects are the most commonly reported in the literature.

Cation ordering

In Ref.,[19] we confirmed that the spinel ferrite $NiFe_2O_4$ possesses a robust inverse Ni/Fe cation distribution between Oh and Td sites and the Ni/Fe cation distribution in the Oh sites corresponding to the space group $P4_122$ (No. 91). This cation ordering was kept constant to build the slabs with the perfect B-terminated surfaces ($Ni_2Fe_2O_8/Fe_2$). With this cation distribution, we furthermore found that the B-terminated surface displays a small band gap of 0.21 eV, resulting from the presence of a charge ordering, which might disappear to the profit of a metallic state at high temperature (see Fig. 6).

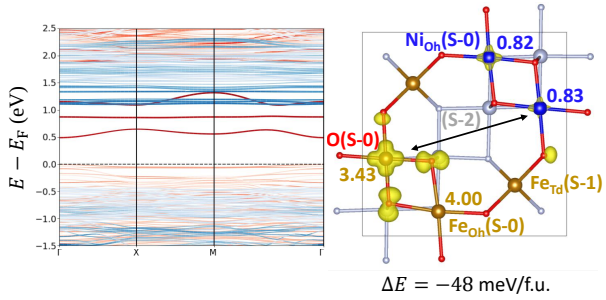

Figure 8: Same as in Fig. 6.a, but for the $(\sqrt{2} \times \sqrt{2})R45°$ $(Ni_2Fe_2O_8)^*/Fe_2$ surface in which Ni and Fe cations have been exchanged, as shown by the double-head arrow in the right subfigure. The total energy ΔE is given according to the energy of the perfect B surface [Fig 6(a)]. The partial charge density (yellow surface) has been calculated for the unoccupied bands located between $E_F + 0.4$ eV and $E_F + 0.7$ eV.

As shown in Fig. 8, by modifying the Ni/Fe cation ordering in Oh sites by swapping one Ni with one of its first-neighbor Fe atoms, we obtain the $(Ni_2Fe_2O_8)^*/Fe_2$ termination, of which the stability is increased by 94 meV per 2 surface f.u, compared to the original B surface. Such a cation swap also results in an increase of the band gap between the valence-band maximum and the lowest unoccupied surface states up to 0.50 eV, which is accompanied by stronger charge localization at the surface, with a larger spin dispropornation between the two Fe atoms, of $\sim 0.57\ \mu_B$, compared to $\sim 0.34\ \mu_B$ with the regular cation ordering (see

Fig. 6 and 8).

The variation of the cation distribution between Td and Oh sites is characterized by the so-called inversion degree λ. Its value depends on the chemical composition, growth conditions and layer thickness, and it can be modified by post-annealing.[59,60] The A termination Ni_2/Fe_4O_8 and the B termination Fe_4O_8/Ni_2 both preserve the stoichiometry of $NiFe_2O_4$, but correspond to the local formation of a normal spinel ($\lambda = 0$) at the surface layer, with the divalent Ni^{2+} cations located in Td sites, while the rest of the spinel structure remains inverse ($\lambda = 1$). The A-terminated Ni_2/Fe_4O_8 surface is one of the most stable terminations, but would require to use oxygen-poor growth conditions, with high temperatures; the B-terminated surface is less likely to be formed. The strong increases of the spin magnetization measured in thin films are often explained in terms of a decrease of the inversion degree,[20,57,58] which could be consistent with the stabilization of the Ni_2/Fe_4O_8 surface. Using ultraviolet photoemission spectroscopy, Lüders, *et al.*,[20] moreover confirmed a non-zero density of states at the Fermi level, in their thin films, which is also in agreement with our calculated metallic surface, originating at the same time from the mixed valence states of Ni cations at the surface (S-0), but also of Fe_{Oh} cations in the subsurface layer (S-1) (see Fig. S3). It is nonetheless important to keep in mind that our structural model remains certainly too simple to completely account for the complexity of a real sample. At the Ni_2/Fe_4O_8-terminated surface, the Ni cations are not anymore in a Td environment and the experimental measurement of a reduced inversion degree would rather refer to the presence of Ni_{Td} cations located deeper in the film. Rather than an increase of the spin magnetization, some studies have reported the appearance of a magnetically-dead layer thin $NiFe_2O_4$ films:[22] in these films, experimentalists measured a change of the inversion degree and the presence of cation vacancies, which may have a strong impact on the magnetic ordering.

Atomic vacancies

The formation of atomic vacancies may strongly affect both the magnetic and conductive properties. In oxygen-poor conditions, previous calculations predicted that neutral oxygen vacancies are the most likely to be present in bulk $NiFe_2O_4$ with the perfect inverse spinel structure, but that these vacancies should not change the spin magnetic moment and only induce the appearance of occupied gap states (resulting from the redistribution of electrons onto surrounding cations) in the band gap near the Fermi level.[19] Recently, we demonstrated that the neutral oxygen vacancies have different consequences when the structure is partially inverse: in that case they can almost totally destroy the band gap and also slightly reduce the spin magnetization.[61] In oxygen-rich conditions, we rather expect the formation of partially-ionized Ni vacancies, which would tend to decrease the spin magnetization; in the presence of these vacancies, the insulating state is preserved, but if the Ni vacancies were neutral, $NiFe_2O_4$ would turn in a hole conductor.[19] Experimentally, oxygen vacancies are common defects in oxides and their formation/disappearance is often proposed to explain the processes of resistive switching, notably in $NiFe_2O_4$-based resistive devices, where they could help creating conductive domains because of the simultaneous formation of Fe^{2+} cations.[11–13] In addition, atomic vacancies have also been proposed to explain the decrease of the magnetization measured in thin films.[21,22]

In the current study, we decided to investigate how vacancies can form in the vicinity of a $NiFe_2O_4$ perfect B surface. To do so, we first calculated the variation of formation energy ΔE_f of one single neutral vacancy located in the successive atomic layers parallel to the surface. The results of these calculations are reported in Table 2; each column is independent and all the energies are given according to the most stable configuration, for a given type of vacancy. In a given atomic layer, when several atomic sites were found non-equivalent, we calculated all the different configurations and only kept the most stable one (see Fig. S5 and Table S2 for more details). Table 2 shows that the different formation energies change monotonously with the distance from the surface layer (S-0).

Table 2: Relative formation energies ΔE_{f} of atomic vacancies V calculated in a slab with two B-type $Ni_2Fe_2O_8/Fe_2$ surface terminations. The energies are calculated as a function of their position to the surface and relatively to the most stable positions.

Layer	ΔE_{f} (eV/vacancy)		
	V(O)	V(Ni)	V(Fe)
S-0	0.00	0.46	1.52 (Py)
S-1			1.11 (Td)
S-2	1.53	0.14	0.40 (Oh)
S-3			0.84 (Td)
S-4	2.53	0.00	0.00 (Oh)

On average, the formation energy of cation vacancies increases from the center of the slab towards the B surface; the energy increase ΔE_{f} is however much larger for Fe atoms, (1.52 eV between S-0 and S-4), than for Ni atoms ($\Delta E_{\mathrm{f}} = 0.46$ eV). As already calculated in bulk $NiFe_2O_4$,[19] these slab calculations confirm that the formation of Fe_{Td} vacancies should be less probable than that of Fe_{Oh} vacancies, which may be in contradiction with some experimental evidence of their presence in thin films.[22] As Fe^{3+}_{Td} cations carry a -5 μ_B spin magnetic moment, if the ferrimagnetic ordering is preserved, creating Fe_{Td} vacancies should increase the spin magnetization.[19] On the other hand, these vacancies also suppress the dominant antiferromagnetic Td-O-Oh interaction, which may destabilize the ferrimagnetic ordering and lead to the formation of magnetically dead layer;[22] our calculations confirm that the effective magnetic interaction is reduced in the presence of Fe_{Td} vacancies even if the ferrimagnetic ordering is preserved for a relatively large amount of vacancies (see Table S1).

The oxygen vacancies show a large variation of their formation energies, of nearly 1.5 eV between the layers S-0 and S-2, and of 2.5 eV between S-0 and S-4. An oxygen vacancy at the B-terminated surface leads to the $Ni_2Fe_2O_7/Fe_2$ termination, which is in the list of the most stable surfaces (see Table 1), and which can be seen in the middle of the stability domain shown in Fig. 2. As explained in the Sec. S.IV of the supplementary information, the oxygen vacancies at the surface are more stable when they involve oxygen sites which are not bound to Fe_{Td}, in agreement with previous findings reported in Ref.[8] As we have seen before for the perfect B-terminated surface, the electronic reconstruction consists in the

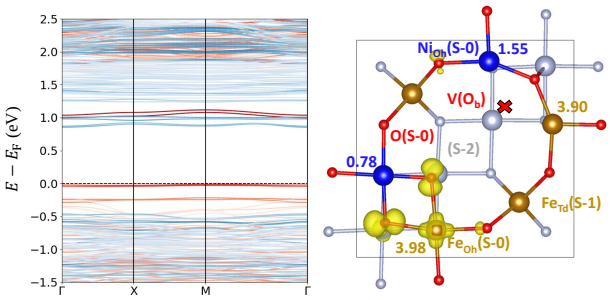

Figure 9: Same as in Fig. 6, but for the $Ni_2Fe_2O_7/Fe_2$ surface, i.e. the $(\sqrt{2} \times \sqrt{2})R45°$ B surface including one oxygen vacancy, represented by the red cross. The partial charge density (yellow surface) has been calculated for the occupied bands located between E_F − 0.1 eV and E_F.

localization of 3 holes at the surface; when a neutral oxygen vacancy is present, two electrons are released, leaving only 1 hole on the Ni_{Oh}(S-0) cation, the furthest from the vacancy, and corresponding to the majority-spin bands with the $d_{x^2-y^2}$ character, ~ 1 eV above the Fermi level. Because of the oxygen vacancy, the ligand hole associated to the majority-spin band just above the Fermi level for the perfect B surface [Fig. 6(a)] disappears to the profit of an occupied band, localized just below the Fermi level and mostly built from the hybridization of $d_{x^2-y^2} + p_x + p_y$ orbitals of atoms far from the vacancy [See Fig. 9]. As a consequence of this less-important surface electronic reconstruction, the reduction of the spin magnetic moment is found lower when an oxygen vacancy is present (-1 μ_B instead of -3 $\mu_B/2$ f.u. for a perfect surface) and thus helps recovering an insulating state with a band gap also close to its bulk value, increasing from 0.21 eV for the perfect B surface without vacancy, up to around 0.9 eV with a vacancy.

In this section, we found that the formation energy of cations and oxygen anions vary in an opposite way as a function of their distance from the surface. It may be claimed that the formation of oxygen vacancies at the surface is energetically effective because of the lesser number of chemical bonds to break. We found that it is particularly true when the oxygen vacancies are located in an atomic site where no Fe_{Td} are present as first neighbors, which concerns half of the 8 surface oxygen sites (see Fig. S5). The number of broken

chemical bonds is not the only parameter which explains the thermodynamic stability of a vacancy, as if it was so, cation vacancies should also preferentially form at the surface, and the competition between the defect- and surface-induced charge reconstructions has also to be considered. Creating neutral oxygen vacancies transfers electrons to the surface and reduces the hole doping. This statement will remain true until the density of neutral oxygen vacancies remains below or equal to 1.5 vacancy per surface of 2 formula units of NFO. Creating neutral cation vacancies will on the contrary transfer more holes to the B-terminated surface; the cations present at the surface will in that case not be in a sufficient number to accommodate all the holes provided by both the surface and the cation vacancies (more particularly if the number of cations is decreased) which may explain why such structural configuration is energetically not favorable.

Conclusion

We performed a numerical investigation of the possible atomic and electronic reconstructions at the $NiFe_2O_4(001)$ surfaces, through the consideration of 27 different terminations. Using *ab initio* thermodynamics calculations, we identified that, among these surface terminations, 9 terminations could be stabilized by a proper selection of growth conditions, while 3 other surface terminations also present low surface formation energies, and could thus be found in real samples, even if metastable.

B-terminated surfaces can be stabilized in oxygen-rich conditions and are expected to be obtained with growth temperatures below 950 K, while A-type surfaces can be obtained otherwise. According to our calculations, we predict that to avoid a reduction of the surface spin magnetization, growth conditions leading to A-type Ni-rich or B-type Fe-rich terminations should be favored.

The stabilization of the B termination obtained from a truncation of the bulk structure, i.e. $Ni_2Fe_2O_8/Fe_2$, should reduce by approximately by 4.38 μ_B nm^{-2} the surface magne-

tization, according to the expected bulk value. This local decrease of the magnetization would result in an electronic reconstruction, associated with hole transfer at the interface, because of the polar character of the $NiFe_2O_4(001)$ layer. The associated surface states are expected to present a small band gap of 0.21 eV at the Fermi level, resulting from a charge ordering, which could disappear at high temperature to the benefit of the appearance of a spin-polarized two-dimensional hole gas. However, the appearance of such a two-dimensional hole gas would be subject to the conditions that the cation ordering in Oh sites is not modified and that the stoichiometry is preserved. We indeed found that a more stable cation distribution is expected to help the surface to recover its insulating character. A good control of the Ni/Fe ratio is also necessary as the perfect B termination is the only one which is close to being metallic, if we discard the surface terminations grown with extreme experimental conditions (like Fe_4O_8/Fe_2 terminations, which would correspond to the formation of hole-doped magnetite Fe_3O_4 on top of the nickel ferrite or the Ni-rich A-type surfaces Ni_2/Fe_4O_8 and $Ni_2/Ni_2Fe_2O_8$, grown at high temperatures). On the contrary to cation vacancies, we calculated that oxygen vacancies are easier to form in the vicinity of B surfaces than in the bulk, in particular at oxygen sites which are not bound to Fe_{Td} atoms. These defects also induce a recovery of the surface insulating state and also diminish the reduction of the surface magnetization, to end with a value close to the bulk.

Our calculations also show that, the formation of a NiO layer on top of the surface, could be possible as its stability domain is close to the bulk one for a large range of oxygen chemical potential; the formation of a FeO layer could on the contrary be possible only in oxygen-poor and iron-rich conditions. The growth of these less-oxidized phases, which does not present any intercalated cations in Td sites, could be facilitated by the low formation energy of oxygen vacancies at surfaces.

Finally, according to our calculations, we predict that surfaces grown under iron-rich ($NiFe_3O_8/Fe_2$ or Fe_4O_8/Fe_2 terminations) or oxygen-poor (every stable A termination, but also surfaces with oxygen vacancies which will counteract the effect of hole transfer) conditons

are suitable to maintain good magnetic properties.

Our results have confirmed the complexity in understanding and controlling the spinel ferrite surfaces. This study is not exhaustive: more complex surfaces could have been envisioned, for example to investigate (i) how the properties change when we vary the density of oxygen vacancies which may tend to segregate at the surface, (ii) if the variation of cation ordering can extend away from the surface, or (iii) the combined effect of cation ordering and oxygen vacancies.[61] It would also be interesting to have a better understanding of other structural parameters such as the film thickness or the in-plane lattice strain, which can result from an epitaxial growth. A logical continuation of this work, focused on bared surfaces, could be to search how their properties could be tuned by using adsorbates or capping layers. Finally, it would be also interesting to calculate how the oxygen vacancies which form at the surface could transfer to the bulk in order to understand the formation of conductive domains during memristive processes.

Acknowledgement

This study has been supported through the ANR Grant ANR-19-CE09-0036. This work was granted access to the HPC resources of CALMIP (Allocation No. 2022-2024/P19004 and P1229).

Supporting Information Available

The following files are available free of charge.

- SI.pdf: A text file divided in 4 sections giving more details about (S.I) the formation energies of all the 27 surface terminations calculated for the study, (S.II) a figure with the layer-resolved DOS calculated for the 12 more stable surfaces, (S.III) the energy differences calculated for different magnetic states at specific surfaces and the the

atomic spin magnetic moments for the most stable surfaces, and (S.IV) some details about how the calculations of the oxygen vacancies have been conducted.

References

(1) Valenzuela, R. Novel applications of ferrites. *Phys. Res. Int.* **2012**, *2012*, 591839.

(2) Moussy, J.-B. From epitaxial growth of ferrite thin films to spin-polarized tunnelling. *J. Phys. D: Appl. Phys.* **2013**, *46*, 143001.

(3) Hirohata, A.; Sukegawa, H.; Yanagihara, H.; Žutić, I.; Seki, T.; Mizukami, S.; Swaminathan, R. Roadmap for emerging materials for spintronic device applications. *IEEE Trans. Magn.* **2015**, *51*, 1.

(4) Parkinson, G. S. Iron oxide surfaces. *Surf. Sci. Rep.* **2016**, *71*, 272.

(5) Pham, T. N.; Huy, T. Q.; Le, A.-T. Spinel ferrite (AFe_2O_4)-based heterostructured designs for lithium-ion battery, environmental monitoring, and biomedical applications. *RSC Adv.* **2020**, *10*, 31622.

(6) Hao, A.; Ning, X. Recent advances in spinel ferrite-based thin films: Synthesis, performances, applications, and beyond. *Front. Mater.* **2021**, *8*.

(7) Mulakaluri, N.; Pentcheva, R.; Scheffler, M. Coverage-Dependent Adsorption Mode of Water on Fe_3O_4(001): Insights from First Principles Calculations. *J. Phys. Chem. C* **2010**, *114*, 11148.

(8) Shi, X.; Li, Y.-F.; Bernasek, S. L.; Selloni, A. Structure of the $NiFe_2O_4$(001) surface in contact with gaseous O_2 and water vapor. *Surf. Sci.* **2015**, *640*, 73.

(9) Hajiyani, H.; Pentcheva, R. Surface termination and composition control of activity of the $Co_xNi_{1-x}Fe_2O_4$(001) surface for water oxidation: Insights from DFT+U calculations. *ACS Catal.* **2018**, *8*, 11773–11782.

(10) Rushiti, A.; Hättig, C.; Wen, B.; Selloni, A. Structure and reactivity of pristine and reduced spinel $CoFe_2O_4$ (001)/(100) surfaces. *J. Phys. Chem. C* **2021**, *125*, 9774–9781.

(11) Hu, W.; Qin, N.; Wu, G.; Lin, Y.; Li, S.; Bao, D. Opportunity of Spinel Ferrite Materials in Nonvolatile Memory Device Applications Based on Their Resistive Switching Performances. *J. Am. Chem. Soc.* **2012**, *134*, 14658.

(12) Tong, S.-K.; Chang, J.-H.; Hao, Y.-H.; Wu, M.-R.; Wei, D.-H.; Chueh, Y.-L. Optimum resistive switching characteristics of $NiFe_2O_4$ by controlling film thickness. *Appl. Surf. Sci.* **2021**, *564*, 150091.

(13) Li, J.; Yao, C.; Huang, W.; Qin, N.; Bao, D. Highly uniform resistive switching properties of $NiFe_2O_4$ films by embedding well-ordered pyramid-shaped Pt/Au nanostructures. *J. Alloys Compd.* **2022**, *890*, 161814.

(14) Tasker, P. W. The stability of ionic crystal surfaces. *J. Phys. C: Solid State Phys.* **1979**, *12*, 4977.

(15) Noguera, C. Polar oxide surfaces. *J. Phys. Condens. Matter* **2000**, *12*, R367.

(16) Ivanov, V. G.; Abrashev, M. V.; Iliev, M. N.; Gospodinov, M. M.; Meen, J.; Aroyo, M. I. Short-range *B*-site ordering in the inverse spinel ferrite $NiFe_2O_4$. *Phys. Rev. B* **2010**, *82*, 024104.

(17) Dey, J. K.; Chatterjee, A.; Majumdar, S.; Dippel, A.-C.; Gutowski, O.; Zimmermann, M. v.; Giri, S. Ferroelectric order associated with ordered occupancy at the octahedral site of the inverse spinel structure of multiferroic $NiFe_2O_4$. *Phys. Rev. B* **2019**, *99*, 144412.

(18) Fritsch, D.; Ederer, C. Effect of epitaxial strain on the cation distribution in spinel ferrites $CoFe_2O_4$ and $NiFe_2O_4$: A density functional theory study. *Appl. Phys. Lett.* **2011**, *99*, 081916.

(19) Sharma, K.; Calmels, L.; Li, D.; Barbier, A.; Arras, R. Influence of the cation distribution, atomic substitution, and atomic vacancies on the physical properties of $CoFe_2O_4$ and $NiFe_2O_4$ spinel ferrites. *Phys. Rev. Mater.* **2022**, *6*, 124402.

(20) Lüders, U.; Bibes, M.; Bobo, J.-F.; Cantoni, M.; Bertacco, R.; Fontcuberta, J. Enhanced magnetic moment and conductive behavior in $NiFe_2O_4$ spinel ultrathin films. *Phys. Rev. B* **2005**, *71*, 134419.

(21) Anjum, S.; Jaffari, G. H.; Rumaiz, A. K.; Rafique, M. S.; Shah, S. I. Role of vacancies in transport and magnetic properties of nickel ferrite thin films. *J. Phys. D: Appl. Phys.* **2010**, *43*, 265001.

(22) Nonaka, Y.; Wakabayashi, Y. K.; Shibata, G.; Sakamoto, S.; Ikeda, K.; Chi, Z.; Wan, Y.; Suzuki, M.; Tanaka, A.; Tanaka, M.; Fujimori, A. Origin of magnetically dead layers in spinel ferrites $M Fe_2O_4$ grown on Al_2O_3: Effects of postdeposition annealing studied by XMCD. *Phys. Rev. Mater.* **2023**, *7*, 044413.

(23) Chang, C. F.; Hu, Z.; Klein, S.; Liu, X. H.; Sutarto, R.; Tanaka, A.; Cezar, J. C.; Brookes, N. B.; Lin, H.-J.; Hsieh, H. H.; et al., Dynamic atomic reconstruction: How Fe_3O_4 thin films evade polar catastrophe for epitaxy. *Phys. Rev. X* **2016**, *6*, 041011.

(24) Arras, R.; Calmels, L. Fully spin-polarized two-dimensional electron gas at the $CoFe_2O_4/MgAl_2O_4(001)$ polar interface. *Phys. Rev. B* **2014**, *90*, 045411.

(25) Kresse, G.; Hafner, J. Ab initio molecular-dynamics simulation of the liquid-metal–amorphous-semiconductor transition in germanium. *Phys. Rev. B* **1994**, *49*, 14251.

(26) Kresse, G.; Furthmüller, J. Efficient iterative schemes for ab initio total-energy calculations using a plane-wave basis set. *Phys. Rev. B* **1996**, *54*, 11169.

(27) Blöchl, P. E. Projector augmented-wave method. *Phys. Rev. B* **1994**, *50*, 17953.

(28) Perdew, J. P.; Ruzsinszky, A.; Csonka, G. I.; Vydrov, O. A.; Scuseria, G. E.; Constantin, L. A.; Zhou, X.; Burke, K. Restoring the density-gradient expansion for exchange in solids and surfaces. *Phys. Rev. Lett.* **2008**, *100*, 136406.

(29) Perdew, J. P.; Ruzsinszky, A.; Csonka, G. I.; Vydrov, O. A.; Scuseria, G. E.; Constantin, L. A.; Zhou, X.; Burke, K. Erratum: Restoring the density-gradient expansion for exchange in solids and surfaces [Phys. Rev. Lett. 100, 136406 (2008)]. *Phys. Rev. Lett.* **2009**, *102*, 039902.

(30) Dudarev, S. L.; Botton, G. A.; Savrasov, S. Y.; Humphreys, C. J.; Sutton, A. P. Electron-energy-loss spectra and the structural stability of nickel oxide: An LSDA+U study. *Phys. Rev. B* **1998**, *57*, 1505.

(31) Monkhorst, H. J.; Pack, J. D. Special points for Brillouin-zone integrations. *Phys. Rev. B* **1976**, *13*, 5188.

(32) Momma, K.; Izumi, F. *VESTA3* for three-dimensional visualization of crystal, volumetric and morphology data. *J. Appl. Cryst.* **2011**, *44*, 1272.

(33) Herath, U.; Tavadze, P.; He, X.; Bousquet, E.; Singh, S.; Muñoz, F.; Romero, A. H. PyProcar: A Python library for electronic structure pre/post-processing. *Comput. Phys. Commun.* **2020**, *251*, 107080.

(34) Reuter, K.; Scheffler, M. Composition, structure, and stability of RuO_2(110) as a function of oxygen pressure. *Phys. Rev. B* **2001**, *65*, 035406.

(35) Hjörvarsson, B.; Pentcheva, R. In *Magnetic heterostructures: Advances and perspectives in spinstructures and spintransport*; Zabel, H., Bader, S. D., Eds.; Springer Berlin Heidelberg: Berlin, Heidelberg, 2008; p 144.

(36) Heifets, E.; Kotomin, E. A.; Mastrikov, Y. A.; Piskunov, S.; Maier, J. In *Thermodynamics*; Moreno-Pirajan, J. C., Ed.; IntechOpen: Rijeka, 2011; Chapter 19.

(37) Osorio-Guillén, J.; Lany, S.; Barabash, S. V.; Zunger, A. Magnetism without magnetic ions: Percolation, exchange, and formation energies of magnetism-promoting intrinsic defects in CaO. *Phys. Rev. Lett.* **2006**, *96*, 107203.

(38) Weast, R. C., Astle, M. J., Eds. *CRC Handbook of Chemistry and Physics*; CRC Press, Boca Raton, 1979.

(39) Jaffari, G. H.; Rumaiz, A. K.; Woicik, J. C.; Shah, S. I. Influence of oxygen vacancies on the electronic structure and magnetic properties of $NiFe_2O_4$ thin films. *J. Appl. Phys.* **2012**, *111*, 093906.

(40) Parkinson, G. S.; Novotný, Z.; Jacobson, P.; Schmid, M.; Diebold, U. A metastable Fe(A) termination at the $Fe_3O_4(001)$ surface. *Surf. Sci.* **2011**, *605*, L42–L45.

(41) Novotny, Z.; Mulakaluri, N.; Edes, Z.; Schmid, M.; Pentcheva, R.; Diebold, U.; Parkinson, G. S. Probing the surface phase diagram of $Fe_3O_4(001)$ towards the Fe-rich limit: Evidence for progressive reduction of the surface. *Phys. Rev. B* **2013**, *87*, 195410.

(42) Gamba, O.; Eder, M.; Poglitsch, M.; Pavelec, J.; Sombut, P.; Meier, M.; Diebold, U.; Schmid, M.; Parkinson, G. S. Formation and stability of Fe-rich terminations of the $Fe_3O_4(001)$ surface. *Mater. Res. Express* **2023**, *10*, 116517.

(43) Pentcheva, R.; Wendler, F.; Meyerheim, H. L.; Moritz, W.; Jedrecy, N.; Scheffler, M. Jahn-Teller Stabilization of a "Polar" Metal Oxide Surface: $Fe_3O_4(001)$. *Phys. Rev. Lett.* **2005**, *94*, 126101.

(44) Bliem, R.; McDermott, E.; Ferstl, P.; Setvin, M.; Gamba, O.; Pavelec, J.; Schneider, M. A.; Schmid, M.; Diebold, U.; Blaha, P.; et al., Subsurface cation vacancy stabilization of the magnetite (001) surface. *Science* **2014**, *346*, 1215.

(45) Koch, F.; Cohen, J. B. The defect structure of $Fe_{1-x}O$. *Acta Crystallogr. Sect. B* **1969**, *25*, 275.

(46) Li, Z.; Lu, J.; Jin, L.; Rusz, J.; Kocevski, V.; Yanagihara, H.; Kita, E.; Mayer, J.; Dunin-Borkowski, R. E.; Xiang, H.; Zhong, X. Atomic structure and electron magnetic circular dichroism of individual rock salt structure antiphase boundaries in spinel ferrites. *Adv. Funct. Mater.* **2021**, *31*, 2008306.

(47) Kuschel, O.; Buß, R.; Spiess, W.; Schemme, T.; Wöllermann, J.; Balinski, K.; N'Diaye, A. T.; Kuschel, T.; Wollschläger, J.; Kuepper, K. From Fe_3O_4/NiO bilayers to $NiFe_2O_4$-like thin films through Ni interdiffusion. *Phys. Rev. B* **2016**, *94*, 094423.

(48) Voogt, F. C.; Fujii, T.; Smulders, P. J. M.; Niesen, L.; James, M. A.; Hibma, T. NO_2-assisted molecular-beam epitaxy of Fe_3O_4, $Fe_{3-\delta}O_4$, and γ-Fe_2O_3 thin films on MgO(100). *Phys. Rev. B* **1999**, *60*, 11193.

(49) Chambers, S.; Thevuthasan, S.; Joyce, S. Surface structure of MBE-grown Fe_3O_4(001) by X-ray photoelectron diffraction and scanning tunneling microscopy. *Surf. Sci.* **2000**, *450*, L273.

(50) Mijiritskii, A.; Boerma, D. The (001) surface and morphology of thin Fe_3O_4 layers grown by O_2-assisted molecular beam epitaxy. *Surf. Sci.* **2001**, *486*, 73.

(51) Yu, L.; Zunger, A. A polarity-induced defect mechanism for conductivity and magnetism at polar–nonpolar oxide interfaces. *Nature Commun.* **2014**, *5*, 15118.

(52) Arras, R.; Gosteau, J.; Huang, D.; Nakamura, H.; Zhao, H. J.; Paillard, C.; Bellaiche, L. Spin-polarized electronic states and atomic reconstructions at antiperovskite Sr_3SnO(001) polar surfaces. *Phys. Rev. B* **2021**, *104*, 045411.

(53) Jacobs, R.; Booske, J.; Morgan, D. Understanding and Controlling the Work Function of Perovskite Oxides Using Density Functional Theory. *Adv. Funct. Mater.* **2016**, *26*, 5471.

(54) Chen, W.-T.; Saito, T.; Hayashi, N.; Takano, M.; Shimakawa, Y. Ligand-hole localization in oxides with unusual valence Fe. *Sci. Rep.* **2012**, *2*, 449.

(55) Łodziana, Z. Surface Verwey transition in magnetite. *Phys. Rev. Lett.* **2007**, *99*, 206402.

(56) Bartelt, N. C.; Nie, S.; Starodub, E.; Bernal-Villamil, I.; Gallego, S.; Vergara, L.; McCarty, K. F.; de la Figuera, J. Order-disorder phase transition on the (100) surface of magnetite. *Phys. Rev. B* **2013**, *88*, 235436.

(57) Rodewald, J.; Thien, J.; Ruwisch, K.; Bertram, F.; Kuepper, K.; Wollschläger, J. Enhanced magnetization of ultrathin $NiFe_2O_4$ films on $SrTiO_3$(001) related to cation disorder and anomalous strain. *Phys. Rev. Mater.* **2020**, *4*, 064404.

(58) Wang, C.; Liu, S.; Shi, J.; Shen, Q. Enhanced magnetic properties of $NiFe_2O_4$ thin films deposited on BCZT-buffered $SrTiO_3$ substrate. *AIP Adv.* **2022**, *12*, 045302.

(59) Sawatzky, G. A.; Van der Woude, F.; Morrish, A. H. Cation Distributions in Octahedral and Tetrahedral Sites of the Ferrimagnetic Spinel $CoFe_2O_4$. *J. Appl. Phys.* **1968**, *39*, 1204.

(60) Hu, G.; Choi, J. H.; Eom, C. B.; Harris, V. G.; Suzuki, Y. Structural tuning of the magnetic behavior in spinel-structure ferrite thin films. *Phys. Rev. B* **2000**, *62*, R779.

(61) Arras, R.; Sharma, K.; Calmels, L. Interplay between oxygen vacancies and cation ordering in the $NiFe_2O_4$ spinel ferrite. *J. Mater. Chem. C* **2024**, *12*, 556.

Graphical TOC Entry